International Journal of Applied Earth Observations and Geoinformation 103 (2021) 102490

Contents lists available at ScienceDirect

International Journal of Applied Earth Observations and Geoinformation

journal homepage: www.elsevier.com/locate/jag

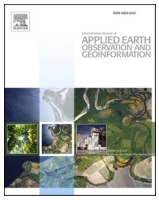

Tracking 21st century climate dynamics of the Third Pole: An analysis of topo-climate impacts on snow cover in the central Himalaya using Google Earth Engine

Abhishek Banerjee [a], Ruishan Chen [a,*], Michael E. Meadows [a,b,c,d], Dhritiraj Sengupta [a], Shray Pathak [a], Zilong Xia [a], Suraj Mal [e]

[a] Key Laboratory of Geographic Information Science, Ministry of Education, School of Geographical Science, Institute of Eco-Chongming, East China Normal University, Shanghai 200241, China
[b] Department of Environmental and Geographical Science, University of Cape Town, Cape Town 7701, South Africa
[c] College of Geography and Environmental Sciences, Zhejiang Normal University, Jinhua 321004, China
[d] School of Geography and Oceanographic Science, Nanjing University, Nanjing 210023, China
[e] Department of Geography, Shaheed Bhagat Singh College, University of Delhi, New Delhi 110017, India

ARTICLE INFO

Keywords:
Snow cover variations
Precipitation and temperature trends
Slope and aspect
Spectral reflectance model
Snow cover-Precipitation-Temperature-Discharge nexus

ABSTRACT

Research on the Himalayan cryosphere has increasingly focused on climate change, considering aspects such as snow cover dynamics, precipitation and temperature trends. The Uttarakhand Himalaya is hydrologically very significant and a more comprehensive understanding of its response to climate change is needed. This paper analyses of elevation-dependent distribution and trends in snow-covered area (SCA), precipitation and temperature for the period 2000–2020 employing MODIS-Terra data, together with reanalysis (CHIRPS) and Landsat-8 data products within the Google Earth Engine (GEE) platform. The study reveals a significant increasing trend in annual, seasonal and monthly precipitation (except November) at different elevations, while SCA and temperatures exhibited more variable trends during the period. Digital elevation and spectral reflectance models reveal the effects of topography and surface attributes on snow cover. Statistical analyses reveal a significant relationship between precipitation and SCA ($R^2 = 0.78$), while seasonal changes in temperature are apparent in an emerging pattern of warmer winters and a cooler pre-monsoon. SCA trends vary markedly between elevation zones in response to precipitation and temperature fluctuations. At higher altitudes, SCA decreased from 2000 to 2020 since, although precipitation increased slightly, marginally higher temperatures led to more snowmelt. Reduced snow cover and increased temperature are also associated with a decline in downstream fluvial during the period for which such data are available (2000 to 2005). The analysis of snow cover dynamics across different elevations improves our understanding of the overall hydrological conditions in the region and enable more reliable flood forecasting and management of water resources.

1. Introduction

The Himalayan mountain region are also known as “the Third Pole” and “water tower of Asia” as it has is extensively snow-covered (You et al., 2020). The region supports the livelihoods of more than 1.8 billion people (~25% of the world population) downstream through its water supply (Kour et al., 2016; Gurung et al., 2017; Sharma et al., 2019; Immerzeel et al., 2020). The Himalayas is a major region of annual snow cover globally (Hori et al., 2017) and have the greatest number and largest area of glaciers (n = 22851; 19428 km^2 respectively) outside the polar regions. These great mountains are the source of ten major river systems, among which are the Ganga, the Indus and the Brahmaputra (Jain et al., 2009), which meet essential water demand for domestic, agricultural, and industrial use in nations including India, Pakistan, Nepal and Bhutan. These developing countries are highly dependent on this water supply as a substantial proportion (70%) of their population is reliant, directly or indirectly, on snow and glaciers melting of the Himalayan mountain regions (Jain et al., 2009). However, due to recent climate changes and temperature increase, much of this system is under serious threat.

* Corresponding author.
E-mail address: rschen@geo.ecnu.edu.cn (R. Chen).

https://doi.org/10.1016/j.jag.2021.102490
Received 7 June 2021; Received in revised form 24 July 2021; Accepted 6 August 2021
Available online 19 August 2021

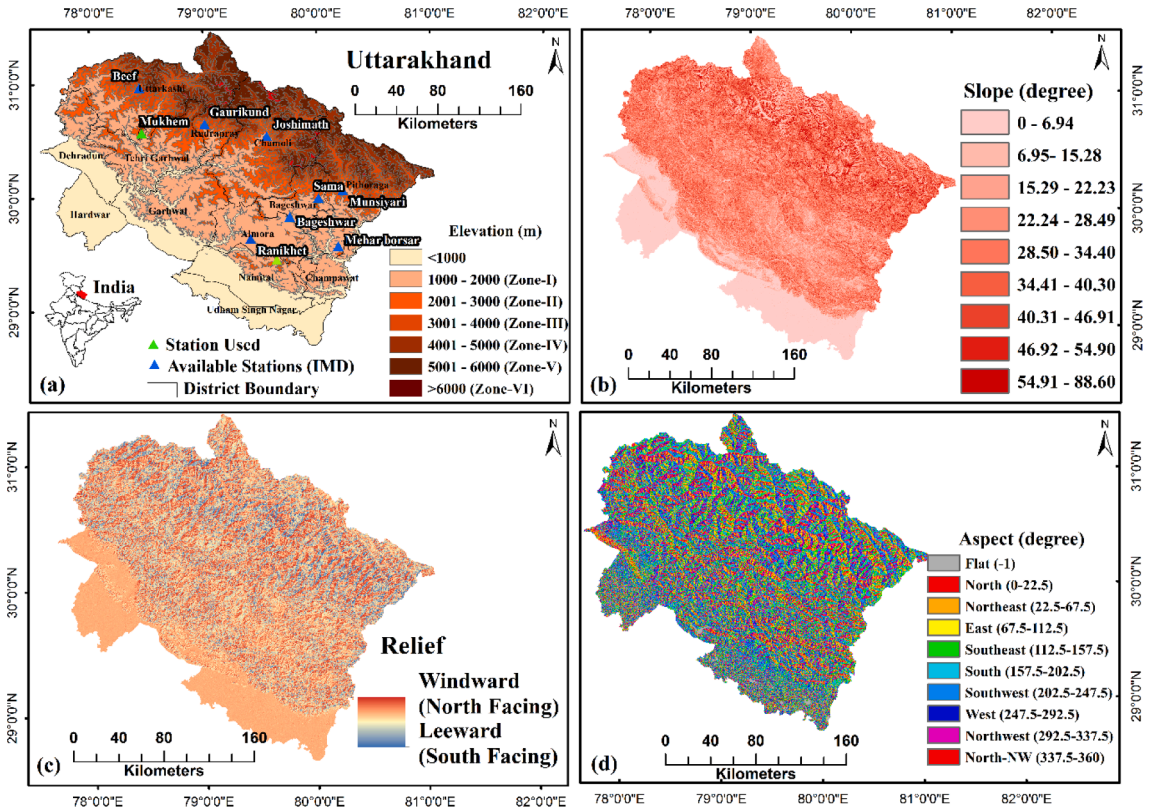

Fig. 1. (a) Classification of elevation into zones with available observed snowfall stations; (b) Slope angle; (c) Relief, showing orientation with respect to predominant wind direction; (d) Slope aspect category.

Table 1
Major topographical characterises of the study area.

Elevation	Area (km^2)	Area (%)	Slope (degree)	Area (%)	Aspect	Area (%)
<1000	13813.83	25.7	0–6.94	17.9	Flat	9.5
1000–2000 (Zone-I)	17508.43	32.6	6.95–15.28	11.2	North	9.5
2001–3000 (Zone-II)	7118.98	13.3	15.29–22.23	14.9	Northeast	9.6
3001–4000 (Zone-III)	4115.42	7.7	22.24–28.49	16.4	East	10.5
4001–5000 (Zone-IV)	5786.79	10.8	28.50–34.40	14.9	Southeast	10.9
5001–6000 (Zone-V)	4915.57	9.2	34.41–40.30	11.5	Southeast	10.1
greater than6000 (Zone-VI)	437.66	0.8	40.31–46.91	7.5	Southwest	10.5
			46.92–54.90	4.0	West	10.2
			54.91–88.60	1.7	Northwest	9.4
					North-northwest	9.9

Source: All the area and percentage were calculated from a reclassified Global Digital Elevation Model (GDEM) (https://earthexplorer.usgs.gov) of the study area

Climate change cascading effects include a reduction in SCA and associated decrease in meltwater discharge which alters the overall water budget of the Himalaya and, in turn, impacts irrigation for agriculture, water supply to cities, hydropower generation, vegetation phenology, food security and social wellbeing (Azmat et al., 2017). Surface reflectance of snow is also used to establish the distribution of snow cover in highland areas. Declining SCA due to a warming climate has an important feedback response. Since darker surfaces are revealed which are then subjected to increased absorption of incoming solar radiation (snow albedo feedback) that increases the surface temperature and in turn accelerates the SCA reduction through melting (Callaghan et al., 2011; Skiles et al., 2018; Das et al., 2020). Many previous studies have reported substantial snow cover reductions with increasing temperature and declining precipitation at the global and regional scale (Singh et al., 2018; Li et al., 2019).

Several studies have noted that the warming trend (~0.9 – 1.6 C) over the last century has been of greater magnitude at higher elevations in the Himalaya than the global mean increase of 0.85 C (Li et al., 2019). In the meantime, the Himalayan population has increased by 250 percent from 19.9 to 52.8 million between 1961 and 2011, which is three times the global average (Apollo, 2017), a situation that accentuates the deleterious influence of climate changes on the livelihoods of people and the ecosystems on which they depend (Aryal et al., 2014). Recent studies have described lower annual and seasonal precipitation in the region due to a reduced temperature gradient between the Indian Ocean and the Tibetan plateau (Palazzi et al., 2013) and increased air

Table 2
Details of data products in this study.

1. Satellite products				
Data	**Data period**	**Resolution**	**Band name**	**Data product**
Snow Cover	Mar 2000-Dec 2020	500 *m*	NDSI_Snow_Cover	MOD10A1 V6 Snow Cover Daily Global 500 *m*
Temperature	Mar 2000-Dec 2020	1000 *m*	LST_Day_1km	MOD11A1.006 Terra Land Surface Temperature and Emissivity Daily Global 1 km
Precipitation	Mar 2000-Dec 2020	0.05-degree arc-second	Precipitation mm/day	Climate Hazards Group InfraRed Precipitation with Station data (V2)
GDEM V2	2011	30 *m*	Elevation model (m, amsl)	ASTER
2. Ground station observations of snow fall				
Name	**Data period**	**Elevation (m, amsl)**	**Location (Lat/long)**	**Data availability (%)**
Ranikheth	1999–2014	1758	29 N and 79 E	6.25
Sama	1998–2014	2506	29 N and 80 E	16.2
Gaurikund	2011–2012	2213	30 N and 79 E	0
Joshimath	1997–2008	2048	30 N and 79 E	6.25
Mukteshwar	1996–2014	2240	29 N and 79 E	63.2
Meher Borsar	2001–2013	1582	31 N and 76 E	0
Munsiyari	1996–2008	2129	30 N and 80 E	20.8
Beef	2010–2014	2708	30 N and 78 E	65
Mukhim	1995–2006	1856	30 N and 78 E	60.4
Bageswar	2000–2012	972	29 N and 79 E	1.92
3. Station discharge data				
Rishikesh	2000–2005	372 *m*	30.09 N and 78.27E	100

Source: All station data were taken from the IMD. Additionally, elevations were established using Google Earth-Pro at each IMD location

temperatures have directly impacted snowfall (Gurung et al., 2011, 2017). Earlier studies have also stated snowfall transformation into precipitation at higher elevation regions, including around Everest, caused by elevation-dependent climate warming (Salerno et al., 2015). Above normal changes in climate parameters significantly affect the spatio-temporal pattern and trends of snowfall, which manifest as reductions of SCA, snow depth, accumulation and melting (Gurung et al., 2017).

A number of studies (e.g. Sharma et al., 2014; Kour et al., 2016; Sahu and Gupta, 2020; Azizi and Akhtar, 2021) in the NW Himalaya, have reported declining SCA in the winter months. Modelled snow cover projections for the western Himalaya also indicate a significant reduction up to 25% by the end of this century with increasing maximum and minimum temperature during autumn and spring season (Nepal et al., 2021). However, there are marked differences depending on locality, as studies in the Karakoram and areas in the upper Indus valley suggest that SCA has actually increased recently (Tahir et al., 2015; Gurung et al., 2017; Ahmad et al., 2019), although in the central Himalaya a strongly negative trend in winter SCA has been reported, along with reduction in spring snow cover in the eastern Himalaya (Gurung et al., 2011). Elevation and topography, including slope angle play an important role in influencing both the direction and scale of SCA distribution and change (Jain et al., 2009; Sharma et al., 2014; Kour et al., 2016).

Since there is currently a paucity of studies concerning SCA and climate in the Uttarakhand (Central) Himalaya, the analysis presented here aims to identify spatial patterns and temporal trends in a range of hydroclimate parameters, *viz*. temperature, precipitation, SCA, and river discharge. By selecting the Uttarakhand Himalaya as a study area, the following objectives for the central Himalaya relating to the period from 2000 to 2020 are established:

1. To map spatial distribution and trends of monthly, annual and seasonal SCA, precipitation and temperature using satellite data products.
2. To assess the effects of elevation, slope and aspect on SCA using a digital elevation model and spectral reflectance model.
3. To establish the spatial nexus between snow cover, temperature, precipitation and river discharge.

2. Characteristics of the study area

The Uttarakhand study domain encompasses a wide sweep of the north-central Himalaya, bordered by Uttar Pradesh (south), Himachal Pradesh (west), Nepal (east) and Tibet (north). The study domain covers an area of more than 53,000 km^2, and extends between 28°43′ to 31°27′N latitude and 77°34′ to 81°02′E longitude (Fig. 1a). Elevation ranges between 184 and 7817 m asl. Topography varies from northern high mountainous ridges and peaks to plains in the south. Around 58 percent of the area is below 2000 m (Fig. 1a, Table 1). Slopes vary from very steep to flat, ranging between 88 and 0°; some 45 percent of the study area lies on steep slopes of between 15 and 45° (Fig. 1b).

The annual mean maximum monthly temperature at the foothills is more than 30 °C, but frequently drops below the freezing point in the winter (DJFM) at high elevations. Mean annual precipitation approximates 1500 mm across the region, although this varies strongly with wind patterns which are in turn influenced by elevation, slope angle, slope aspect, and overall orientation of the mountains (Fig. 1) (Sharma et al., 2014). Maximum precipitation generally occurs during the monsoon season (JAS) (Banerjee et al., 2020). Winter precipitation (DJFM) which occurs due to the westerly disturbances (WDs) is, however, also a significant contributor to annual totals, especially at higher elevations where it produces snow. The high mountainous region of Uttarakhand is vulnerable to climate change which has already exhibited accelerated glacier melting (Mal et al., 2019), increasing river discharge and more frequent flash floods (Allen et al., 2015). The Uttarakhand has a total population of ~ 10 million, which is second highest among the Himalayan states of India (Census of India 2011). The region experienced population growth of 18.8% between 2001 and 2011 and, in terms of natural resources, also support 580 million people the adjacent Ganga basin lowlands (Jain et al., 2009). It is expected that the population of the study area will increase to ~ 13 million by 2036 (Census of India 2011) and major rivers like the Ganga, having capacity to fulfil demands (social-economic development and daily purposes) of more 70% people downstream with fresh water from snowmelt runoff (30–40%) (Chowdhury et al., 2021), these combinations of environmental factors add further weight to the need to understand longer-term variations in the climate of the region.

3. Database

Both surface observation station and remote sensing data products processed using GEE platform were utilised in this study, with sources, availability and limitations described below.

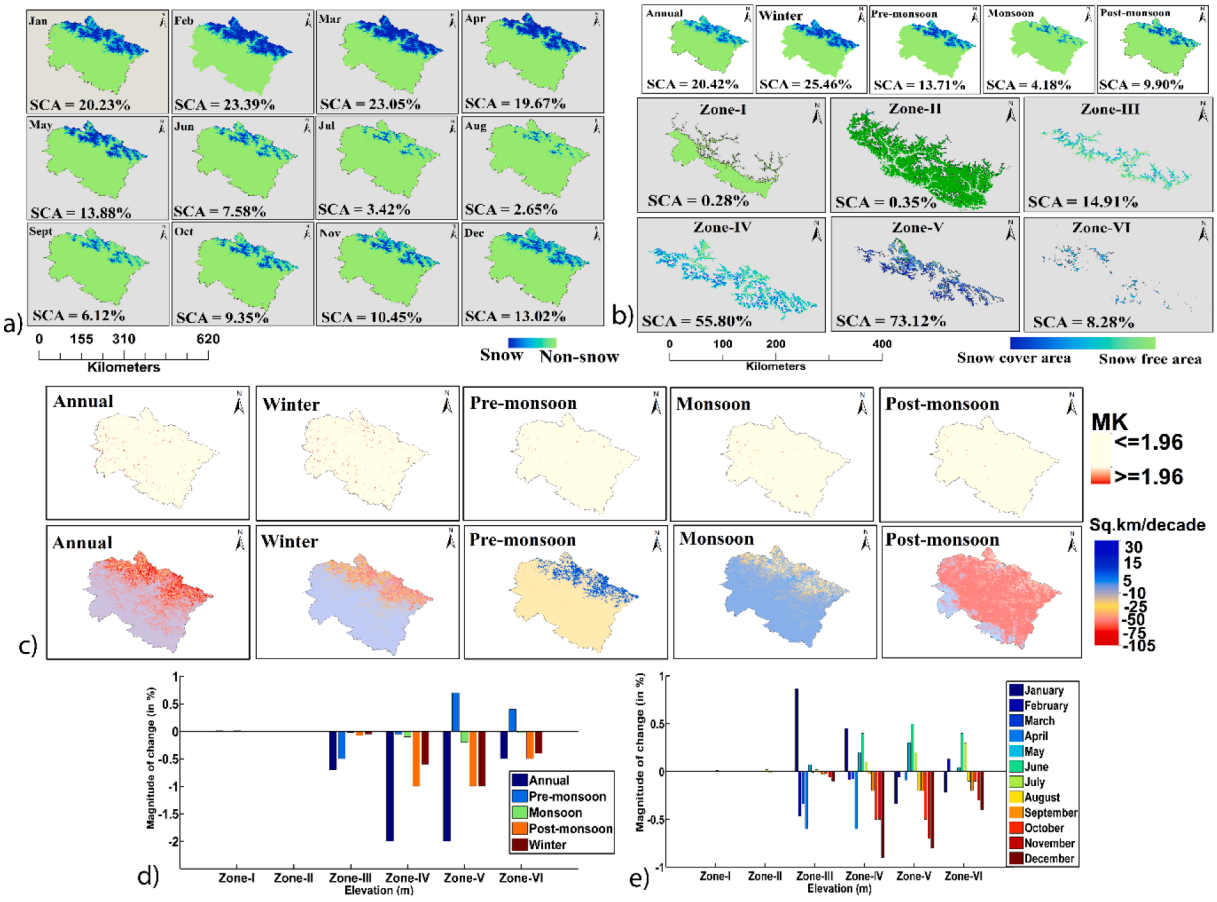

Fig. 2. (a) Spatio-temporal distribution of mean monthly SCA; (b) Distribution of mean annual and seasonal SCA; (c) Spatio-temporal trends of SCA with level of significance (α = <0.05) and actual magnitude of change; (d and e) Annual, seasonal and monthly magnitude of changes as % of SCA.

3.1. Remote sensing data handling

3.1.1. MODIS snow cover (2000–2020)

The Moderate Resolution Imaging Spectroradiometer (MODIS) version 6 (MOD10A.006-Terra) daily snow product data, covering the period between 2000 and 2020 at a spatial resolution of 500 m were selected to investigate spatio-temporal distribution and temporal trends (Hall and Riggs, 2016; Eythorsson et al., 2019). The US National Snow and Ice Data Center provides an extensive series of MODIS scenes for snow estimation in a sinusoidal projection, which was then processed using the powerful computational system of GEE (Eythorsson et al., 2019; Notarnicola, 2020). The sinusoidal projection was transformed to WGS-84 for the study region in the GEE-Application Programming Interface (GEE-API). The MOD10A.006-Terra product has maximum snow coverage mainly in the mountain regions throughout years at higher spatio-temporal scale (Sahu and Gupta, 2020).

3.1.2. Modis LST (2000–2020)

The MOD11A1 V6 Terra Land Surface Temperature (LST) and Emissivity daily day time product was utilised to estimate the surface temperature of the study area at 1000 m spatial resolution (Table 2). These data comprise both Terra and Aqua platforms to obtain day and night time temperature values, although we did not use MODIS-Aqua, because of low temporal resolution (July 2002) and previously observed consistency issues with band 6 (Eythorsson et al., 2019; Sahu and Gupta, 2020). This product has been widely calibrated with ground measurements, including in the Himalayan region (Mishra et al., 2014). However, Kenawy et al. (2019) report that the occurrence of heavy aerosols loading in the atmosphere may influence results and in order to account for this, we made monthly and seasonal mean composites of the image collections which were then clipped to the study area using GEE.

3.1.3. Chirps precipitation data (2000–2020)

We used the Climate Hazards Group InfraRed Precipitation with Station Data Version 2.0 (CHIRPS-V2.0) (Ullah et al., 2018) which yields daily data at high spatial (0.05-degree arc-second) and temporal (1981 to present) resolution along with quasi-global coverage (50°S to 50°N). CHIRPS is a data reanalysis product and very close match with observed stations, which integrates satellite precipitation records, large scale observational station data, and several climatological datasets to provide extended spatial and temporal coverage (Ullah et al., 2018; Banerjee et al., 2020; Wang et al., 2021). Shrestha et al. (2017) noted that CHIRPS daily data performs better in higher elevation regions especially since 1992 due to a correcting applied to spatial bias, although the dataset reportedly overestimate precipitation amounts due to the presence of snow, ice and cold cloud (Banerjee et al., 2020).

3.1.4. Digital elevation model (DEM)

The Advanced Spaceborne Thermal Emission and Reflection Radiometer (ASTER) Global Digital Elevation Model Version 2 (GDEM V2) was obtained for this study from NASA LP DAAC data portal at 30 m spatial resolution. The ASTER GDEM V2, has 260,000 more stereo-paired images than the earlier version, and enables enhanced spatial coverage, while reducing the incidence of vertical and horizontal errors (Mishra et al., 2014) so we used this also to determine slope angle, aspect and elevation zones of the study area. Jarihani et al. (2015) reported on the capacity of open-source DEMs and found higher spatial accuracy of ASTER GDEM for hydrological measurements, while Costa et al. (2019) report the limitations of freely available DEMs in lacking optimal spatial resolution.

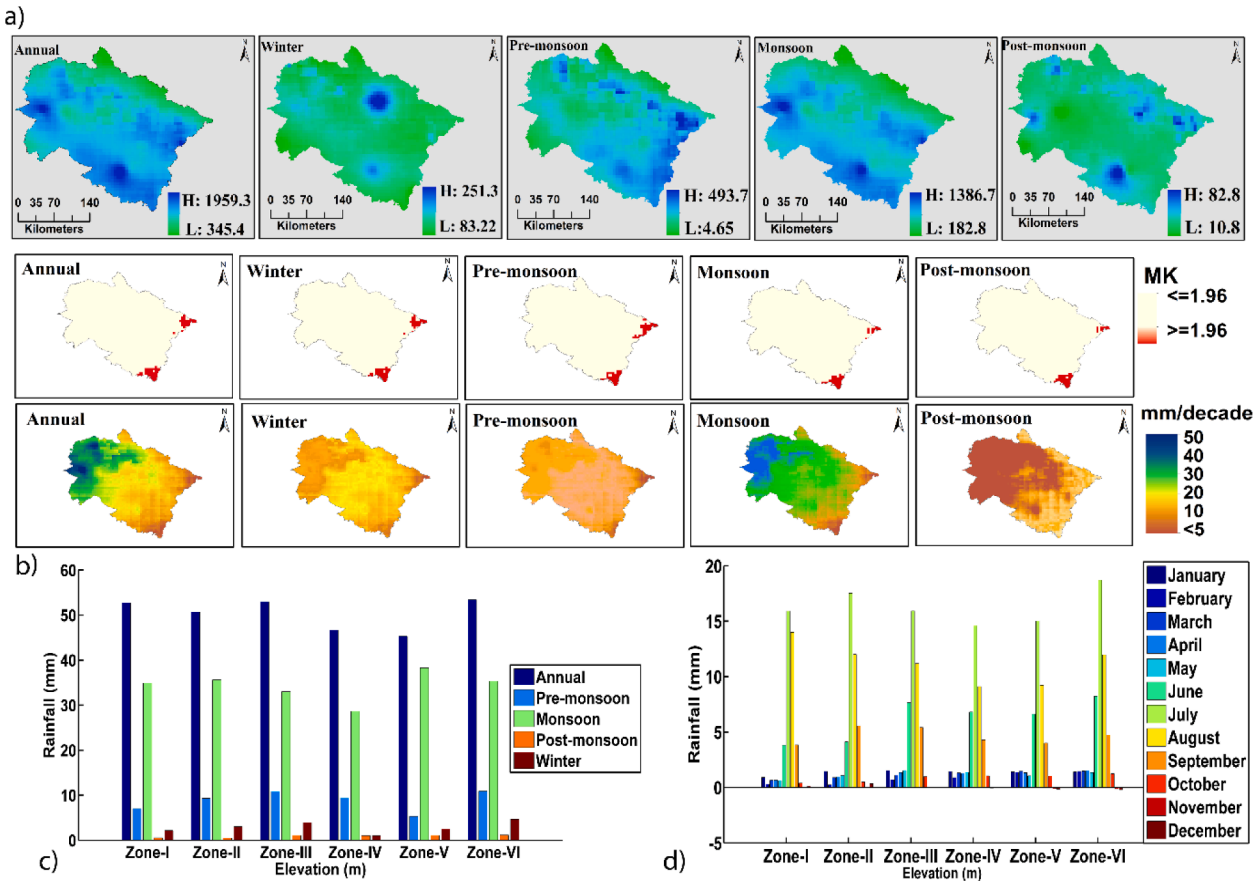

Fig. 3. (a) Spatio-temporal distribution of mean annual and seasonal precipitation; (b) Spatio-temporal trends of precipitation with level of significance ($\alpha = <0.05$) and actual magnitude of change; (c and d) Annual, seasonal and monthly magnitude of change.

3.2. Ground observation station records

The availability of ground observed data in mountainous terrain is a challenge due to remoteness, inaccessible topography and extreme weather conditions. However, ground station records of snowfall were available from the India Meteorological Department (IMD) for eight surface observatories within the region. However, due to inconsistency and completeness of long-term records, only two stations with at least 60 percent data coverage for the period 2000 to 2005 were available to authenticate the MODIS snow product (Table 2) (Gurung et al., 2011). Monthly discharge data for the Rishikesh gauging station on the Ganga river, regrettably only covering the period 2000 to 2005, were obtained from the Uttarakhand state irrigation authority and used to validate inter-correlation between climate variables and river discharge.

4. Methods: Image processing, model setup, spatial nexus and statistical applications

4.1. SCA delineation

It is now widely accepted that GEE offers a highly effective means of processing large-scale geospatial data by minimising the effects of data handling challenges, as well as solving issues related to the local availability of high computational capacity (Sánchez-Ruiz et al., 2019; Amani et al., 2020). Employing several GEE functions provided via JavaScript API code editor, and minimising the effect of cloud cover, we obtained composite monthly, seasonal and annual mean imageries representing of the Normalised Difference Snow Index (NDSI) using snow cover band of the MOD10A1.006 Terra Snow Cover Daily Global 500 m product. This provides a detailed estimation of snow cover on a scale ranging between 0 and 100 (Hall and Riggs, 2011; Notarnicola, 2020) (Code-1). NDSI values greater than 40 are classified as snow cover using the '.gt' function which returns the first value greater than the second after applying 'least cloudy pixel extraction' technique in GEE. Addition to this, daily precipitation and temperature distribution data were also collected using GEE. Thereafter, the bicubic interpolation technique was applied to all datasets (MODIS snow, LST and CHIRPS) to transform them into a common spatial scale (Banerjee et al., 2020).

Recent studies assessed the MODIS snow cover product to be 90–93 percent accurate in detecting snow in mountain areas (Hall and Riggs, 2016; Sahu and Gupta, 2020). The product may underestimate SCA at higher elevations in the presence of dense alpine forest (Mishra et al., 2014), but this is not the case in the present study because there is very limited vegetation cover above 3000 m. Again, cloud cover in such regions is known to affect SCA detection and may result in overestimation (Snapir et al., 2019). It is possible to calibrate the MODIS snow product against ground station data using statistical procedures after segregating the SCA as suggested by Misra et al. (2020) where temperature $\leq 0\,^{\circ}C$ is treated as the condensation point for snow and precipitation. Thereafter, various statistical indices with uncertainty facilitated validation including A1) Correlation Coefficient (CC), A2) Root Mean Square Error (RMSE), A3) Mean Bias Error (MBE), A4) Mean Absolute Error (MAE) A5) Probability of Detection (POD), A6) False Alarm Ratio (FAR), A7) Critical Success Index (CSI), A8) Accuracy, A9) Probability of False Detection (POFD), A10) Success Ratio (SR) and A11) Bias indices (Tran et al., 2019; Sánchez-Ruiz et al., 2019) are used here (Supplementary Appendix-A) for the period of 2000 to 2005, based on available observed data. The validation was conducted to confirm the appropriateness of MODIS data as a tool to estimate SCA in situation where observation station data are scarce due to inaccessible terrain and inhospitable

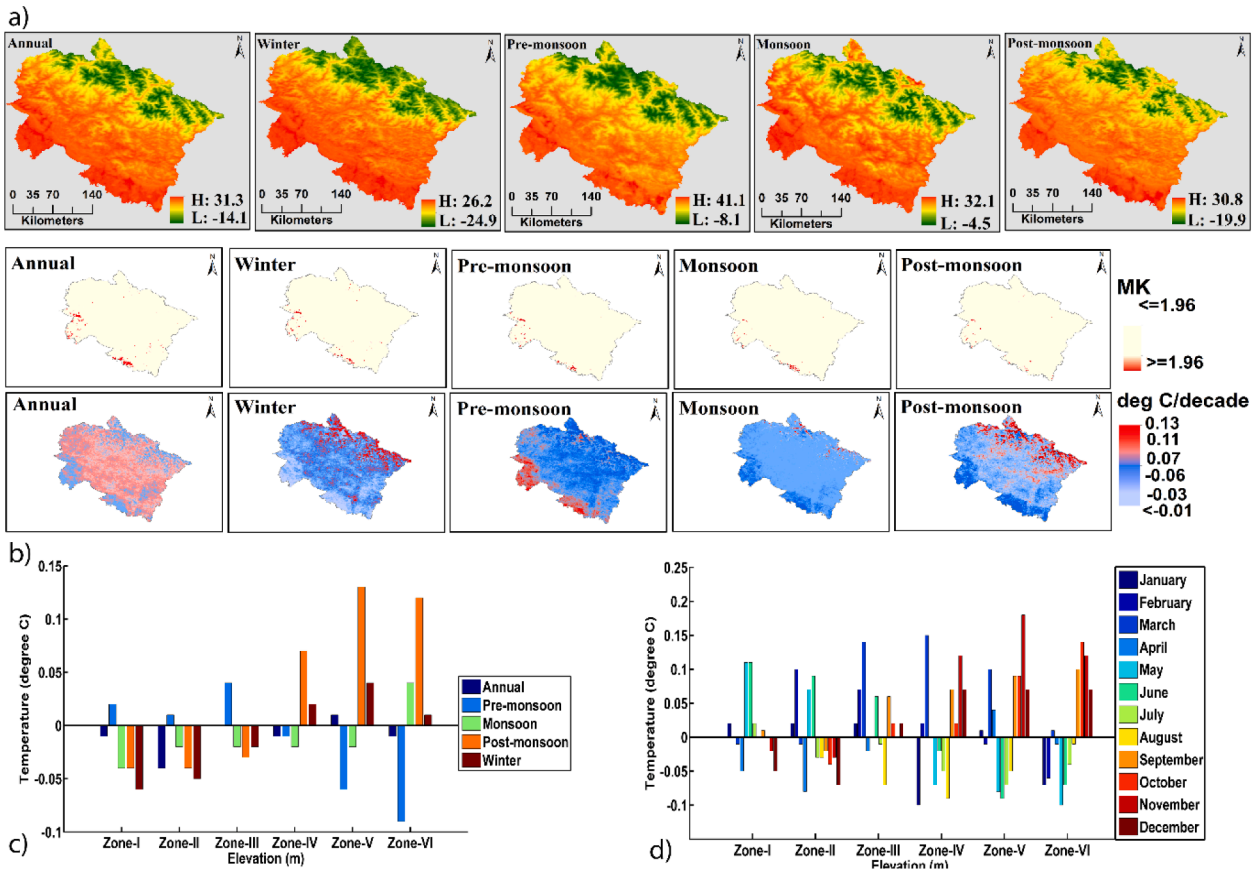

Fig. 4. (a) Spatio-temporal distribution of mean annual and seasonal temperature; (b) Spatial trends of temperature; with level of significance (α = <0.05) and actual magnitude of change; (c and d) Annual, seasonal and monthly change.

climate.

To facilitate the seasonal analysis, monthly data were aggregated for pre-monsoon (April-May-June), monsoon (July-August-September), post-monsoon (October-November) and winter (December-January-February-March) following the scheme used in other studies (Jain et al., 2009; Kour et al., 2016).

4.2. Long-term trend analysis

We employed the Lag-1 autocorrelation (alpha < 0.05) to test the serial-correlation in long-term datasets to limit the effect of positive auto-correlation in the long-term spatio-temporal trend (Tahir et al., 2015; Banerjee et al., 2020). The relationship between temporal patterns of snow cover and meteorological variables was assessed using Sen's slope estimator (B2) to evaluate the scale of trends and the Mann-Kendall (MK) (B1) test to evaluate their statistical significance at the 95% confidence level (Code-2) (Notarnicola, 2020; Azizi and Akhtar, 2021) (Supplementary Appendix-B).

4.3. Elevation, slope angle and aspect

The GDEM image was classified to generate slope angle, aspect and elevation zones of the study area using ArcGIS 10.1. Seven-elevation zones, nine-slope angle and ten-slope aspect categories were identified (Table 1). These slope angle and aspect maps were then compared with the annual NDSI image using the Map Algebra tool in ArcGIS 10.1. Furthermore, these were reclassified to estimate the nature of the relationship between SCA and topographical characteristics.

4.4. Spatial correlation between SCA and climate variables

Pixel-wise spatial correlation between snow cover, river water discharge and climate variables at the 95 percent significance level was performed in the GEE platform using Pearson's correlation coefficient (Code-3), where the values vary between + 1 to −1 to indicate the direction and strength of the relationship (Sazib et al., 2018).

4.5. Spectral reflectance model

Modelling of multiple topographic elements along with the spectral reflectance was carried out using Google Earth Explorer and MATLAB programming language (R2019a). Elevation, slope and aspect data were calculated from ASTER DEM at 30 m spatial resolution and two Landsat 8-OLI orthorectified scenes for winter (22–03-2019) and summer (10–06-2019) seasons available in Google Earth Explorer and further processed using MATLAB programming language after applying the 'CFMask' cloud-removal algorithm (Stillinger et al., 2019). A total of 16,000 pixels within the study domain was plotted on a scatter graph to illustrate the influence of topographic factors on SCA distribution.

4.6. Identifying the relationships between SCA, climate variables and discharge

To investigate the relationships between SCA, precipitation, temperature and discharge, normalised deviation and linear regression methods were used (alpha < 0.05) following standardisation of all data for bringing them into a single unit and appropriate value limits. Spatial regression was employed using the MATLAB programming language only for the period 2000 to 2005, based on the limited availability of discharge data (Tahir et al., 2015; Azmat et al., 2017).

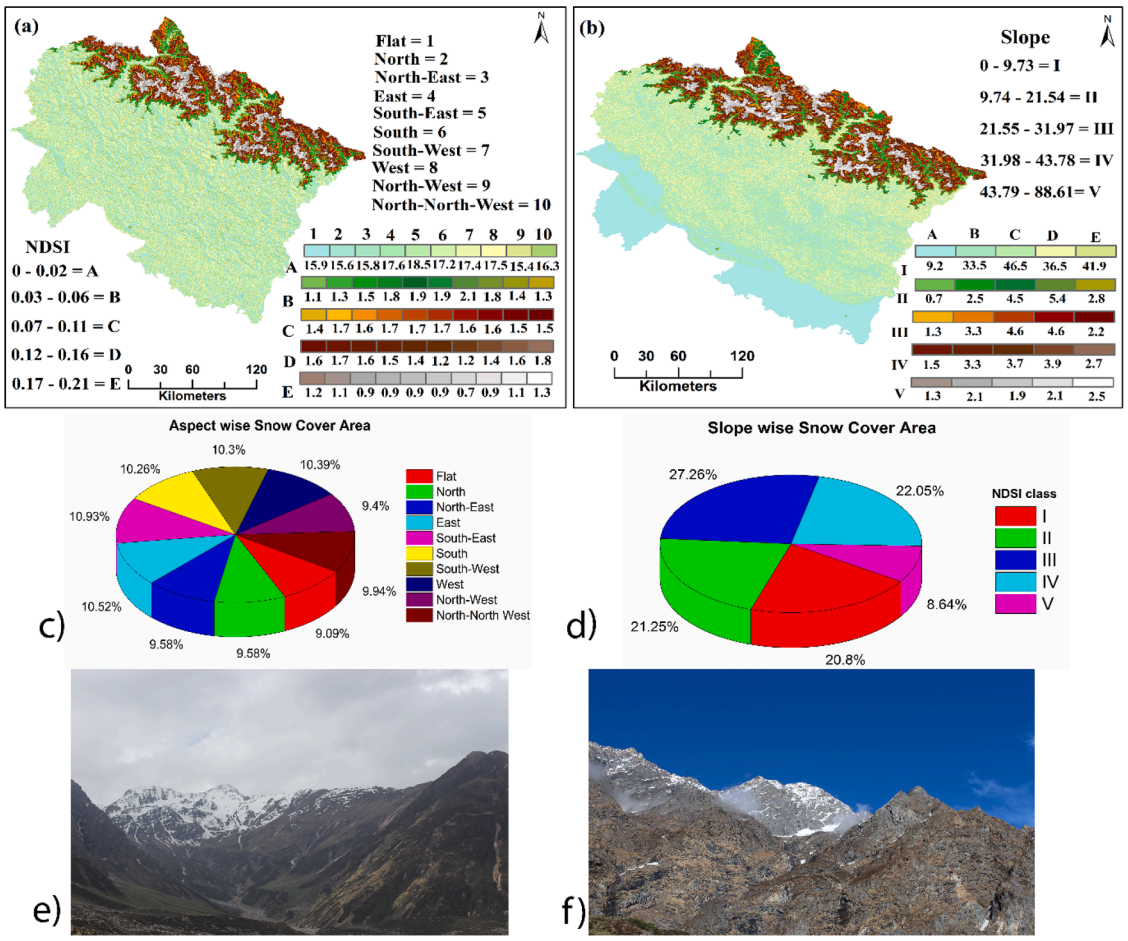

Fig. 5. Snow cover distribution in relation to (a) Aspect and (b) Slope angle. Pie-diagrams (c and d) show percentage distribution of SCA according to Aspect and Slope respectively. Photos: (e) and (f), show SCA variation with aspect and slope. (Photographs by A.B. during a field visit in July 2016).

5. Results

5.1. Validation of the MODIS product through statistical applications

The strength of the correlation between observed snowfall and MODIS-SCA (where temp ≤ 0 °C) is key to whether or not the satellite product can be used reliably to reveal temporal trends. After applying numerous statistical indices (Supplementary Table 1), it emerges that MODIS snow cover data are indeed well suited to the detection of snow cover distribution throughout the study area. A strong spatial correlation exists between observed snowfall and SCA detected by MODIS ($R^2 = 0.83$ for Mukhim and mean $R^2 = 0.76$ across the two ground observatories). According to RMSE, MODIS-Terra product slightly overestimate snow counts at lower elevation regions (RMSE of Mukhteswar = 13.6 mm, uncertainty ± 0.9), where high elevation chunks having relatively less systematic error compared with ground observations (RMSE = 8.9 mm, uncertainty ± 0.6). In addition, MODIS-Terra sensor has less mean bias error in relation to station data, averaging 0.96 mm. Snow cover values for both observed stations and MODIS data products are spatially similar revealed by other descriptive indices (POD = 1). Again, as compared with ground stations, MODIS data performed effectively in detecting snow at Mukhim (CSI = 0.62), although it yields an underestimation at Mukhteswar. MODIS snow product has the capacity to capture actual snow by minimising the effects of overestimation, as FAR and SR values are below 0.3 for both observed stations. Spatial bias between observed and MODIS data products is lower at Mukhim (1.3), but comparatively higher at Mukhteswar (1.5), which reinforces that MODIS-Terra sensor has ample capacity to detect SCA in the higher elevation regions. Overall, the statistical analyses illustrate the effectiveness of MODIS in accurately detecting SCA in the study area.

5.2. Elevation dependent distributions and trends

5.2.1. SCAs

The effect of elevation on annual, seasonal and monthly SCA for the period from 2000 to 2020 is illustrated in Figure S1 ($R^2 = 0.73$; $p < 0.05$). Maximum SCA was observed in Zone-V and Zone-IV during the winter and pre-monsoon seasons, with mean annual coverage of 73.1 and 55.8 percent, respectively (Fig. 2b). Maximum SCA therefore occurred from December to March during the study period, averaging 10697 km^2 (Fig. 2a). Lower elevation regions generally experience less snow cover throughout the year (Fig. 2b). Furthermore, elevation-dependent spatio-temporal long-term annual, seasonal and monthly trends of SCA vary over time as illustrated in Fig. 2c. Although statistically not significant, in general, there appears to be a marginal increase in annual snow cover across lower elevations (Zone-I and II) and rapid decline across the higher elevation regions (Zone-III to VI), averaging −36.8 km^2/decade (Fig. 2c). However, there are marked contrasts between seasons and between different elevation zones. For example, there are quite substantial annual reductions in SCA at higher elevations (Zones IV to VI), both in absolute area and proportional to the size of the zones (Fig. 2d). SCA in Zones IV and V was respectively more than 100 km^2 and 90 km^2 less in 2020 compared to 2000, much of this a consequence of reduced values in the months that characterise the post-monsoon and winter seasons (Fig. 2c Annual snow cover reduction

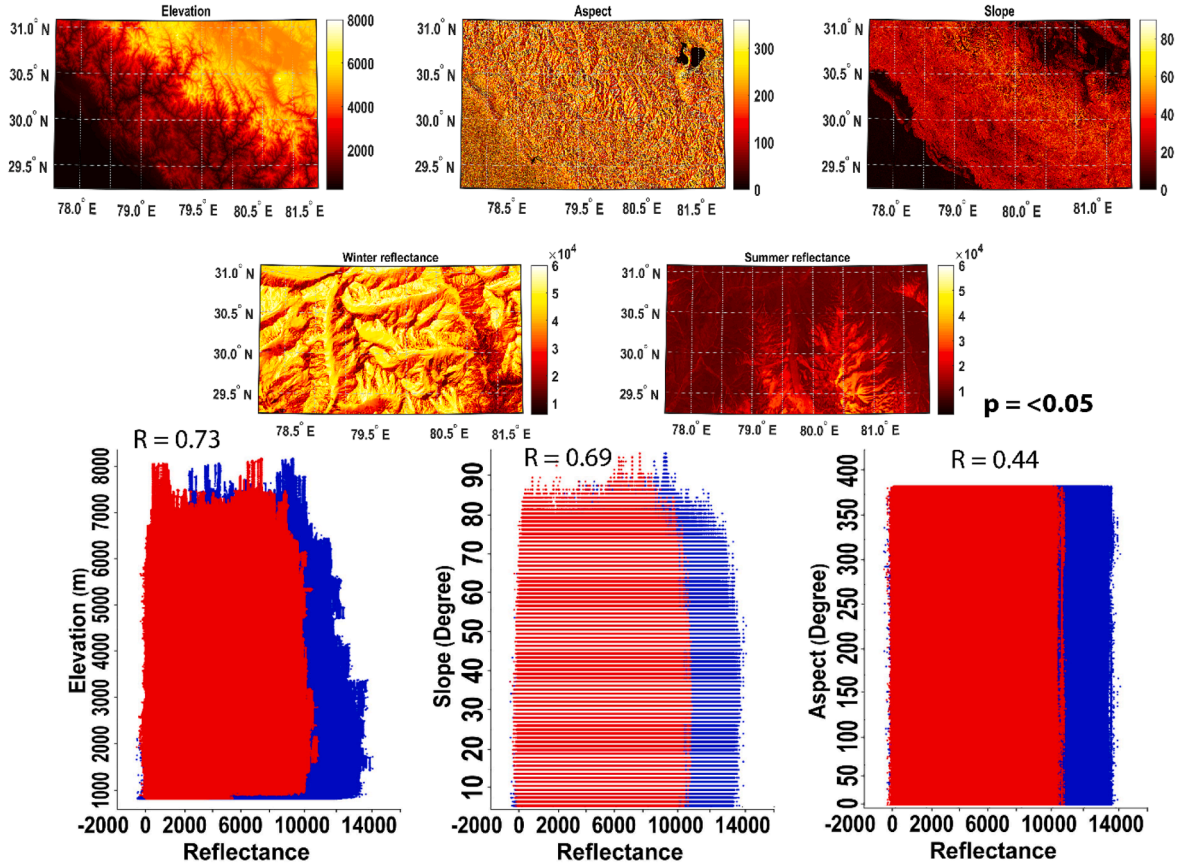

Fig. 6. Upper panel show modelled distribution map of elevation, aspect, slope and summer-winter reflectance of snow. Lower panel showing, pixel to pixel scatter plot of elevation, slope and aspect with corresponding snow cover for summer and winter. Red represents summer and Blue winter snow reflectance. Both tasks were performed using GEE Explorer (https://explorer.earthengine.google.com/#workspace) and MATLAB programming language. (For interpretation of the references to colour in this figure legend, the reader is referred to the web version of this article.)

would be even greater in Zone V if it were not for the pre-monsoon season, which recorded an increase over the period (Fig. 2c, d).

5.2.2. *Precipitation*

Precipitation in the study region is spatially and seasonally variable as affected by local elevation and physiography ($R^2 = 0.4$; $p < 0.05$, Fig. S2). Our findings clearly depict a two-step precipitation distribution according to altitude. Initially, when monsoon precipitation advances towards the northwest, the lower Himalayan foothills witness maximum precipitation in Zone-I. Thereafter, there is an abrupt increase in Zones-II and III related with orographic effects. Furthermore, Fig. 3a illustrates that the southern and south-eastern areas of the region are generally wetter and the southwestern parts are comparatively drier. Seasonally, these zones receive most of their precipitation during the monsoon and pre-monsoon, averaging 940 mm (Fig. 3a) influenced by the Indian Summer Monsoon (ISM). High elevation regions receive significant amount of precipitation during the winter season (in the forms of snow, when temperatures are ≤ 0 °C) (Fig. 3a) sourced from the WDs. Fig. 3b illustrates spatio-temporal trends, including that precipitation increased especially in the western part of the Uttarakhand, over 19 years (Fig. 3b) and is a characteristic of all elevation zones. Precipitation in Zones-I, III and VI was observed to increase by, on average, 53.05 mm/decade, while values in Zone-II, IV and V were augmented by 47.55 mm/decade. A statistically significant increasing trend across all elevation zones is evident during the monsoon season, averaging up to 34.29 mm/decade, particularly in Zones-I, II and III (Fig. 3b). Significantly higher precipitation is also a feature of the pre-monsoon, winter and post-monsoon seasons (Fig. 3c). The most prominent increases were observed for the summer period, June to September (9.60 mm/decade), more especially in July when precipitation increase exceeded 16 mm/decade. Indeed, increasing precipitation throughout the period (2000 to 2020) characterised all months (averaging 4.09 mm/decade) except for November, which was marginally drier (-0.06 mm/decade; Fig. 3d).

5.2.3. *Temperature*

As expected, temperature is strongly influenced by elevation (Fig. S3, $R2 = 0.93$; $p < 0.05$). The highest mean annual temperature was observed in the lower elevation regions, averaging 31.8 °C, whereas considerably lower temperatures were recorded at higher altitudes, averaging −2.4 °C in Zone VI (Fig. 4a) in accordance with the lapse. Seasonally, maximum temperature observed during pre-monsoon season (33.9 °C) followed by monsoon (28.1 °C), post-monsoon (24.9 °C) and winter (21.3 °C). Further analysis of altitude-dependent trends in annual temperature for the last two decades reveals a slightly cooler conditions across all elevation zones, although this is not statistically significant (-0.01 °C/decade; Fig. 4b). There are, however, some strong seasonal contrasts evident. For instance, while there is a trend towards slightly lower temperature in lower elevation zones through most seasons, there are more strongly positive shifts in the post-monsoon season for Zones IV, V and VI (Fig. 4c). The higher elevation zones are associated with marked inter-seasonal variability in temperature trends (Fig. 4c). For example, in Zones V and VI especially, the trend has been towards decreasing temperatures trends in the pre-monsoon sooner, but increasing temperature in the post-monsoon months (Fig. 4c-d).

5.3. *Spatial relationships between SCA and topographic variables*

The distribution of SCA with slope angle and aspect is shown in

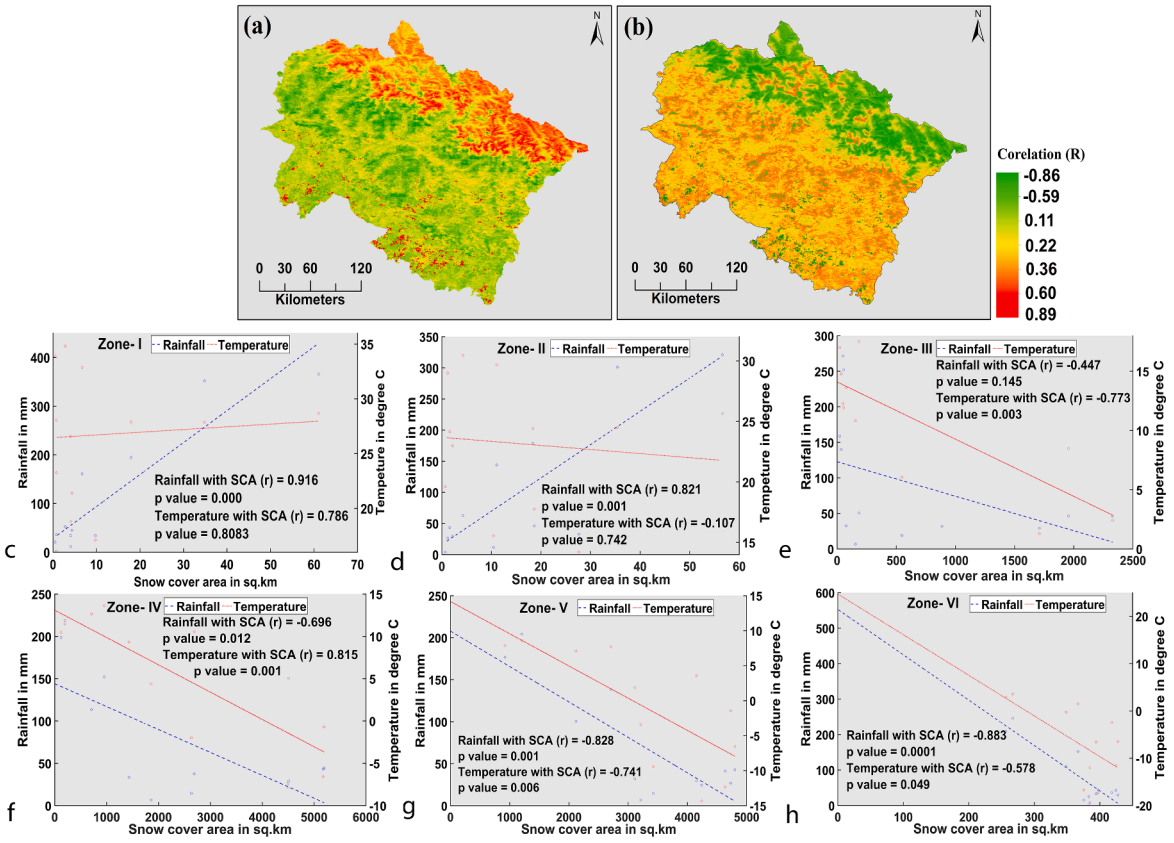

Fig. 7. Spatial correlation between; (a) Precipitation and snow cover; (b) Temperature and snow cover from 2000 to 2020; (c to h) Elevation-dependent relationship between SCA, precipitation and temperature.

Fig. 5a-b, revealing that topography exerts a strong influence on snow cover distribution in the Uttarakhand Himalaya. Slope category-III (21.55–31.91°) record maximum snow cover (61.2 km^2) during the period 2000 to 2020, followed by slopes in categories IV, II and I. SCA is influenced by slope aspect in that maximum snow cover was observed in southwest and west-facing surfaces (Fig. 5c) followed by the east, southeast oriented slopes (Fig. 5d). Fig. 5f illustrates how steeper slopes limit snow cover, while Fig. 5e depicts the greater accumulation of SCA on south-easterly facing slopes, due to less solar radiation (Mountain shadow zone).

Results from the spectral reflectance model reveal the effects of topography on SCA distribution. Due to variation in surface topography and weather conditions, remotely sensed (Landsat-8) snow reflectance data for two different seasons were collected and calibrated, revealing strong spatial relationships between SCA distribution and elevation, slope and aspect. The reflectance model shows that SCA is largely dependent on elevation ($R^2 = 0.73$, $p < 0.05$) and slope ($R^2 = 0.69$, $p < 0.05$), while aspect exerts moderate influence (Fig. 6). The spatial model further reveals that maximum snow is observed between 3000 and 4000 m elevations on slopes with 30 to 60-degree surface alignment.

6. Discussion

6.1. Temporal trends in SCA, precipitation and temperature (2000–2020)

Our study reveals significant reductions in mean annual SCA and an increase in precipitation during the period between 2000 and 2020, while temperatures exhibit rather more variability and are largely altitude-dependent. This paper highlights the effects of elevation on regional climate anomalies and its associated changes with regards to interactions between elevation, varied topography, precipitation and temperature which appear to affect both the intensity and spatio-temporal distribution of SCA. Although SCA is shown to have generally been decreasing over the period 2000–2020, lower elevation regions (Zone-I and II), do exhibit marginal increase, probably because of higher precipitation (Tahir et al., 2015). The IPCC 5th report (Hartmann et al., 2013) also states an increase in SCA caused by higher annual precipitation during the past few decades for this region, which is also supported by a recent study by Hori et al. (2017). Higher elevation areas (Zone-V and VI) experienced positive anomalies in SCA only during the pre-monsoon season possibly attributable to the declining temperature trend and more frequent WDs responsible for the solid precipitation as proposed by others (Cannon et al., 2015; Gurung et al., 2017; Bilal et al., 2019). According to recent studies (Dimri et al. 2015, Midhuna et al 2020), there is a marginal shift in the WDs linked to the westerly jet stream (during winter season) and associated precipitation from winter towards the pre-monsoon season, concurring with our finding of increasing SCA anomalies in this season. Increase winter temperatures at high elevations (0.12 °C/decade) coupled with relatively lower precipitation (11.2 mm/decade) precipitated a marked declining trend in SCA (-58.3 km^2/decade). This also indicates a clear seasonal shift in snow precipitation and hence its accumulation from winter to the pre-monsoon season, a feature also reported recently in several studies in the central Himalayan regions (Bhutiyani et al., 2010), while Pepin et al. (2015) suggest that this is a characteristic of higher mountains globally.

The present study points to a declining trend in SCA at higher elevations, especially in the post-monsoon and winter months, which may be accounted for by the shift to relatively warmer air and surface temperatures in these seasons (Krishnan et al., 2019), although from February to April increasing snow accumulation coincides with somewhat lower temperatures in these months (Bormann et al. 2018; Daloz

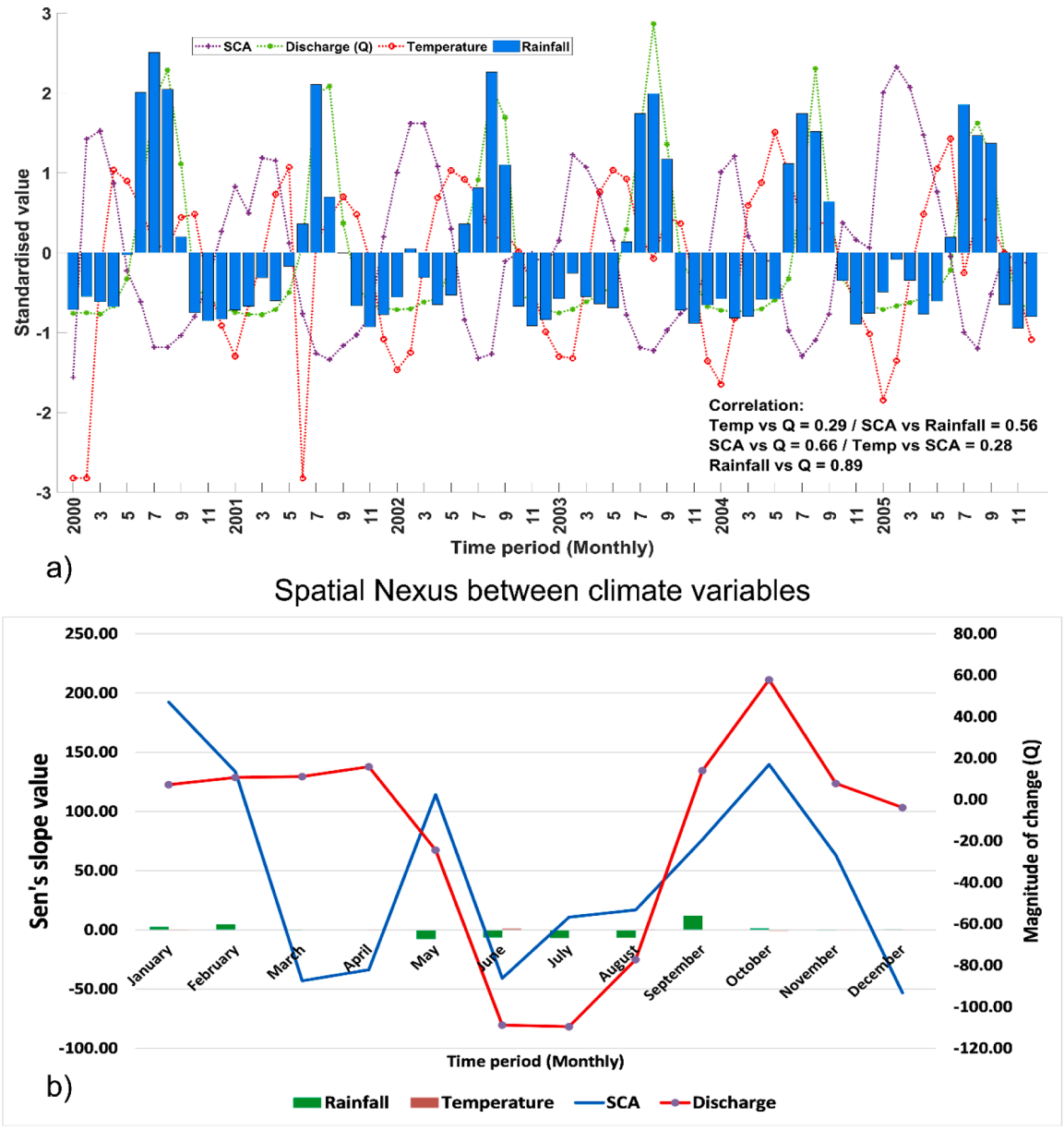

Fig. 8. (a) Correlation between standardised precipitation, temperature, SCA and discharge during 2000–2005. Coefficient were subject to statistical significance test (α = <0.05), (b) Spatial relationship of climate variables using Sen's slope estimator (α = <0.05).

et al. 2020). Azmat et al. (2017) have reported declining SCA up to 2009, although this trend reversed in the past decade due to an increase in precipitation and lower air temperatures. A complex of feedback effects, involving temperature, precipitation and snow cover, occur in the Himalayan region due to its complex topography and vast east–west dimension, together with the variable influence of global, regional and local atmospheric processes. As recorded in this study, increasing precipitation trends are apparent across most seasons for the entire study area, which is a commonly observed recent pattern in the western Himalayas (Mishra et al., 2014; Tahir et al., 2015), and may be attributed to an increasing frequency and/or magnitude of Indian Ocean Dipole (IOD), WDs, and cloudburst (Gurung et al., 2017). Positive and negative IODs have significant bearings on the Indian monsoon, thereby affecting precipitation amount and intensity in the Himalayas. During the positive/negative IODs, the monsoon precipitation is observed to be strong/weak (Sahu et al. 2012). A weaker monsoon in the Indian sub-continent is believed to lead to extreme weather events in the central Himalaya as most of the moisture-bearing monsoonal winds then fail to penetrate the western Himalaya and drop their precipitation in the central Himalayas (Karki et al., 2017). Moreover, observed increased temperatures in the Pamir mountain and Tibetan area intensify the ISM, enhancing moisture transfer and deep convection in the Himalayan foothills (Tahir et al., 2015). Anthropogenic activities such as, tourism, road construction, hydropower projects, expansion of agricultural lands and consequent prolonged human presence higher up in the snow-dominated alpine valleys of the Himalaya have also significantly influenced SCA in the region by promoting its earlier melting (Aryal et al., 2014).

6.2. *Variations in SCA, precipitation and temperature with elevation and topography*

6.2.1. *Elevation*

Precipitation has increased significantly during the study period in all elevation zones (p= <0.05), while temperature and SCA exhibit less consistent trends, supported by the recent study of Tahir et al. (2015) in

the river basins of the western Himalaya. The spectral reflectance model reveals that SCA is strongly dependent on elevation, followed by aspect and slope angle. Sharma et al. (2014) and Gurung et al. (2017) also reported a robust spatial correlation between SCA and altitude. Our study reveals maximum snow cover in Zones-IV and V, although there was a slight downward trend in the lower zones due to an increase in pre-monsoon temperature and less frequent snowfall in recent years. Azmat et al. (2017) reported that snowfall increased at altitudes 2000 m to 4000 m in north-central Himalaya between 2000 and 2014, but decrease above 4000 m, which they attributed to increasing precipitation in the middle portion of the western Himalayan region. In this study, the lower elevation regions (Zone-I, II and III) experienced a marginally increased SCA coincident with higher precipitation and lower temperatures coupled with the effects of the two-step precipitation distribution based on the abrupt increase in altitude and relief (Bookhagen and Burbank, 2006).

6.2.2. Aspect and slope

This study has highlighted the importance of topography in influencing SCA, which is also noted by recent studies of Sharma et al. (2014) and Mishra et al. (2014). We show that maximum annual SCA is found on south-east and east-facing slopes at angles between 20 and 30°mainly due to the solar radiation effect. West and north-west facing slope have less SCA due to longer duration of solar radiation resulting rapid faster snowmelt, as noted also by Misra et al., (2020). Singh et al. (2018) reach a similar conclusion, with maximum SCA on the east and south-east facing slopes in the north-western Himalaya. Jain et al. (2009), on the other hand, report that more than 40 percent of the SCA in the Satluj river basin was found on southwest to north-facing slopes. Seasonal contrasts in SCA with slope are also apparent, as also noted by Sharma et al. (2014). Maximum SCA in gentle slope (Class-II and III) and its gradual decrease with increased slope angle, as reported here, lead to more frequent avalanches on steep topography (Misra et al., 2020). In addition, slopes in class I and II are associated with less SCA, again due to surface orientation effects.

6.3. The SCA-Precipitation-Temperature-Discharge nexus

The pixel by pixel spatial relationships between SCA and precipitation (Fig. 7a), SCA and temperature (Fig. 7b) are shown from 2000 to 2020. Not surprisingly, as shown in Fig. 7c-e, and also noted by Tahir et al. (2015) in the Astore River basin, of northwestern Himalaya, higher temperatures reduce SCA. A statistically significant positive relationship ($R^2 = 0.86$) between SCA and precipitation is also evident. The inverse spatial relationship between SCA and temperature at higher elevations (Zones III to VI, Fig. 7 e-h) occurs since monsoon precipitation does not usually reach beyond 4500 m, and therefore SCA is not directly related to precipitation above this altitude, especially during the monsoon season (Chen et al., 2018). Reduced SCA exposes darker surfaces that can absorb relatively more incoming solar radiation, thereby resulting in further heating of the land surface and is thus a positive feedback mechanism (Callaghan et al., 2011; Skiles et al., 2018). Moreover, results suggest an increased proportion of precipitation with a higher mean temperature that, when falling directly on snow, directly reduces SCA (Callaghan et al., 2011). In contrast, winter snowfall occurs during WDs which are strongly influenced by orientation, elevation and slope. Northwest facing slopes receive heavier snowfalls than those oriented to the southeast, as during winter season (Indian Winter Monsoon), the WDs, with moisture sourced from the north Atlantic Ocean, approach from a north-westerly direction and, due to Himalayan orographic effects, may produce heavy precipitation. This process is intensified and accelerated due to the presence of the westerly jet stream (Dimri et al., 2015; Midhuna et al 2020). Increased annual precipitation at lower elevation regions, when surface temperatures are below 0 °C, may result in more SCA which is akin to the pattern observed in eastern Tibet (You et al., 2020). Karki et al. (2020) suggest a cooling phenomenon in the winter season in the Himalayan foothills that accounts for increased SCA at lower altitudes. Remarkably, the pre-monsoon season, the warmest season of the year, exhibits an increase in the SCA above 4000 m asl, which may be attributed to both cooling (-0.08 °C/decade) and an increase in precipitation (~8.0 mm/decade) (Figs. 2-4). WDs are most prevalent in the winter months, but have been shown by Dimri et al., (2015) to becoming more frequent in the pre-monsoon season because of its seasonal shift, leading to an increase in snowfall and hence the SCA.

For the period 2000 to 2005, Fig. 8a illustrates the strong correlation between temperature (negative) and precipitation (positive) with SCA, averaging 0.61. Similar pattern was reported by Tahir et al. (2015) and Azmat et al. (2017) who highlighted the importance of increasing precipitation in lower and middle elevation regions on snow cover distribution. Our study documents a decreasing temperature trend for winter months in the region (-0.06 °C/decade), a phenomenon also observed in the lower elevation zones in the adjacent Himalayan mountain region of Nepal (Karki et al., 2020) associated with statistically significant increasing SCA. This has important implications for river discharge, since this is strongly dependent on snow cover and snowmelt. Only a relatively weak correlation is observed between monthly temperature and discharge ($r = 0.29$) while precipitation and discharge are significantly ($r = 0.89$) correlated, especially during the monsoon months (Fig. 8a). SCA is significantly correlated with discharge during the snowmelt period ($r = 0.66$), which suggests an increasing discharge with melting snow during summer season (MJJA). However, Azmat et al. (2017) recorded a negative relationship between discharge and precipitation in the western Himalaya related to decreasing SCA from 2000 to 2009, but a positive correlation between temperature and discharge. This pattern was also observed in the northwestern Himalayan region by Bhutiyani et al. (2008), and in the Himalaya of Nepal by Mishra et al. (2014). The results conform to the observation that 50 percent of the total annual discharge of the northwestern Himalayan rivers is snowmelt water (Mukhopadhyay and Khan, 2014).

Until now, the complex linkages between temperature, precipitation, SCA and fluvial discharge have not previously been well established for the central Himalaya. Fig. 8b depicts the 'nexus' that characterises these parameters as evident during for the period 2000–2005. A marked decline in precipitation and SCA from May to August is followed by a pronounced decrease in river discharge. However, Jasrotia et al. (2021) have used regional climate models to predict increasing precipitation and associated river discharge until 2080, followed by a slight decrease to 2100. This emphasises (Ahmad et al., 2019) the strong influence of climate variations on water availability for the highly populated regions reliant on these resources. Several other studies have shown how large-scale global climate shifts, such as frequency and magnitude variations in El-Niño and changes in the strength of teleconnections between the Indian Ocean and Tibetan plateau, in addition to marked land use alteration, influence downstream water resources in the region (Palazzi et al 2013; Banerjee et al., 2020).

7. Conclusions

The spatial and temporal changes of snow cover distribution (MODIS-Terra) in relation to precipitation (reanalysis: CHIRPS), temperature (MODIS-Terra), topography (ASTER GDEM) and river discharge (station observed) in the central Himalaya are presented here for the period 2000 and 2020. The study concludes the following.

1. The study demonstrates the proficiency of MODIS-Terra snow cover data to estimate snow detection at high-elevations where availability of station observed data is a major challenge. Spatio-temporal trends in SCA and other meteorological parameters from 2000 to 2020 using MODIS-Terra and reanalysis datasets reveal changes in annual, seasonal and monthly SCA that are explained by variations in precipitation and temperature. These trends are shown to be strongly elevation-dependent. At lower elevations in the study area (Zone-I

and II), SCA increased marginally in response to higher precipitation and lower air temperatures, whereas, at higher elevation (Zone-IV to VI), increased temperatures (0.12 °C/decade) and relatively lower precipitation (11.2 mm/decade) have led to strongly reduced SCA.
2. Elevation plays an important role in climate and impacts snow accumulation, in the study area. Snow cover is more prominent at higher elevation (about 65%). Maximum SCA was found on the south (10.52%) and east-facing (10.26%) slopes. The highest precipitation occurred in the lower and middle elevation regions. Statistical analysis using the spatial reflectance model and several other descriptive statistical applications revealed the degree to which snow cover varies with elevation, slope and aspect.
3. Analysis of the spatial nexus between SCA, precipitation, temperature, and discharge indicate a strong spatial correlation between a) increased precipitation and increasing SCA ($R^2 = 0.6$) at a lower elevation, b) increasing precipitation and increasing discharge ($R^2 = 0.9$), and a moderate correlation between c) decreasing temperature and increasing SCA ($R^2 = 0.3$) during the pre-monsoon season at higher elevations, and d) decreasing temperature and increasing discharge ($R^2 = 0.3$).
4. Results also show that the remotely sensed data products reliably reflect ground observations in remote mountainous areas and that GEE is a powerful tool to collate and establish spatio-temporal variations in different variables.

The overall findings of this study inform water resource management plans in a region characterised by a complex set of relationships between precipitation, temperature, snow cover and river discharge. During this era of rapid climate change (both natural and anthropogenic) it is important that future studies should incorporate these factors in developing a more complete scenario of spatio-temporal climate dynamics of the Himalayan region.

CRediT authorship contribution statement

Abhishek Banerjee: Conceptualization, Methodology, Formal analysis, Software, Validation. **Ruishan Chen:** Funding acquisition, Conceptualization, Project administration, Supervision. **Michael E. Meadows:** Writing – original draft, Resources, Supervision, Validation. **Dhritiraj Sengupta:** Data curation, Software, Visualization. **Shray Pathak:** Validation. **Zilong Xia:** Software, Visualization. **Suraj Mal:** Conceptualization, Supervision.

Declaration of Competing Interest

The authors declare that they have no known competing financial interests or personal relationships that could have appeared to influence the work reported in this paper.

Acknowledgements

We gratefully acknowledge to the MODIS-Terra sensor data together with NOAA, NCDC, UCSB and Climate Hazard Groups for providing long-term gridded high-resolution datasets. Additionally, we are thankful to IMD, Pune for providing station observed snowfall data. We greatly appreciate the insightful and constructive comments from anonymous reviewers and the editor which have assisted in improving the scientific integrity of the manuscript.

Funding

This study was conducted with the support of the Second Tibetan Plateau Scientific Expedition and Research Program - STEM (2019QZKK0906), the National Key Research and Development Program of China (2017YFC1503001), the National Social Science Fund of China (20ZDA085), the National Natural Science Foundation of China [grant number 41771119], the Research Fund of the Geological Mineral Resources and Environmental Exploration Program [DD20190427], and funding from Institute of Eco-Chongming (IEC). AB and SM are grateful to the HINEX project for supporting the fieldwork for the present study.

Appendix A. Supplementary data

Supplementary data to this article can be found online at https://doi.org/10.1016/j.jag.2021.102490.

References

Ahmad, M., Alam, K., Tariq, S., Blaschke, T., 2019. Contrasting changes in snow cover and its sensitivity to aerosol optical properties in Hindukush-Karakoram-Himalaya region. Sci. Total Environ. 699, 134356 https://doi.org/10.1016/j.scitotenv.2019.134356.

Allen, S., Rastner, P., Arora, M., Huggel, C., Stoffel, M., 2015. Lake outburst and debris flow disaster at Kedarnath, June 2013: hydro meteorological triggering and topographic predisposition. Landslides 13, 1479–1491. https://doi.org/10.1007/s10346-015-0584-3.

Amani, M., Ghorbanian, A., Ahmadi, S.A., Kakooei, M., Moghimi, A., Mirmazloumi, S.M., et al., 2020. Google Earth Engine Cloud Computing Platform for Remote Sensing Big Data Applications: A Comprehensive Review. IEEE: J. Sel. Top. Appl. Earth Obs. Remote Sens. 13, 5326–5350. https://doi.org/10.1109/JSTARS.2020.3021052.

Apollo, M., 2017. Mountaineer's waste: past, present and future. Ann. Valahia Univ. Targovista Geogr. Ser. 16, 13–32. https://doi.org/10.1515/avutgs-2016-0002.

Aryal, A., Brunton, D., Raubenheimer, D., 2014. Impact of climate change on human-wildlife-ecosystem interactions in the Trans-Himalaya region of Nepal. Theor. Appl. Climatol. 115, 517–529. https://doi.org/10.1007/s00704-013-0902-4.

Azmat, M., Liaqat, U.W., Qamar, M.U., Awan, U.K., 2017. Impact of changing climate and snow cover on the flow regime of Jhelum River. Western Himalaya. Reg. Environ. Change 17, 813–825. https://doi.org/10.1007/s10113-016-1072-6.

Azizi, A.H., Akhtar, F., 2021. Analysis of spatiotemporal variation in the snow cover in Western Hindukush-Himalaya region. Geocarto Int. https://doi.org/10.1080/10106049.2021.1939442.

Banerjee, A., Chen, R., Meadows, M.E., Singh, R.B., Mal, S.M., Sengupta, D., 2020. An analysis of long-term rainfall trends and variability in the Uttarakhand Himalaya using Google Earth Engine. Remote Sens. 12, 709. https://doi.org/10.3390/rs12040709.

Bhutiyani, M.R., Kale, V.S., Pawar, N.J., 2008. Changing streamflow patterns in the rivers of northwestern Himalaya: Implications of global warming in the 20th century. Curr. Sci. 95 (5).

Bhutiyani, M.R., Kale, V.S., Pawar, N.J., 2010. Climate change and the precipitation variations in the northwestern Himalaya: 1866–2006. Int. J. Climatol. 30, 535–548. https://doi.org/10.1002/joc.1920.

Bilal, H., Chamhuri, S., Mokhtar, M.B., Kasturi, D.K., 2019. Recent snow cover variation in the Upper Indus basin of Gilgit Baltistan. Hindukush Karakoram Himalaya. J. Mt. Sci. 16 (2), 296–308. https://doi.org/10.1007/s11629-018-5201-3.

Bookhagen, B., Burbank, D.W., 2006. Topography, relief, and TRMM-derived rainfall variations along the Himalaya. Geophys. Res. Lett. 33 https://doi.org/10.1029/2006GL026037.

Bormann, K.J., Brown, R.D., Derksen, C., Painter, T.H., 2018. Estimating snow-cover trends from space. Nat. Clim. Chang. 8, 924–928. https://doi.org/10.1038/s41558-018-0318-3.

Callaghan, T.V., Johansson, M., Brown, R.D., et al., 2011. Multiple effects of changes in Arctic snow cover. Ambio 40, 32–45. https://doi.org/10.1007/s13280-011-0213-x.

Cannon, F., Carvalho, M.V., Jones, C., Bookhagen, B., 2015. Multi-annual variations in winter westerly disturbance activity affecting the Himalaya. Clim. Dyn. 44, 441–455.

Census of India. 2011. Population projections for India and States 2011-2036. Report of the technical group on population projections. Ministry of Health and Family welfare, Govt. of India. https://nhm.gov.in/New_Updates_2018/Report_Population_Projection_2019.pdf.

Chen, R., Chuntan, H., Liu, J., Yang, Y., Liu, Z., Wang, L., Kang, E., 2018. Maximum precipitation altitude on the northern flank of the Qilian Mountains, northwest China. Hydrol. Res. 49(5), 1696-1710. doi:10.1038%2Fs41598-017-05345-6.

Choudhury, A., Yadav, A.C., Bonafoni, S., 2021. A response of snow cover to the climate in the Northwest Himalaya (NWH) using satellite products. Remote Sens. 13, 655. https://doi.org/10.3390/rs13040655.

Costa, R., Mazzoli, P., Bagli, S., 2019. Limitations posed by free DEMs in watershed studies: The sase of river Tanaro in Italy. Front. Earth Sci. 7, 141. https://doi.org/10.3389/feart.2019.00141.

Daloz, A.S., Mateling, M., Ecuyer, T.L., Kulie, M., et al., 2020. How much snow falls in the world's mountains? A first look at mountain snowfall estimates in A-train observations and reanalyses. The Cryosphere. 14, 3195–3207. https://doi.org/10.5194/tc-14-3195-2020.

Das, S., Giorgi, F., Giuliani, G., 2020. Investigating the relative responses of regional monsoon dynamics to snow darkening and direct radiative efects of dust and carbonaceous aerosols over the Indian subcontinent. Clim. Dyn. 55, 1011–1030. https://doi.org/10.1007/s00382-020-05307-1.

Dimri, A.P., Niyogi, D., Barros, A.P., et al., 2015. Western Disturbances: A review. Rev. Geophys. 53, 225–246. https://doi.org/10.1002/2014RG000460.

Eythorsson, D., Gardarsson, S.M., Ahmad, S.K., Hossain, F., Nijssen, B., 2019. Arctic climate and snow cover trends – Comparing Global Circulation Models with remote sensing observations. Int J Appl Earth Obs Geoinf. 80, 71–81. https://doi.org/10.1016/j.jag.2019.04.003.

Gurung, D.R., Kulkarni, A.V., Giriraj, A., Aung, K.S., Shrestha, B., Srinivasan, J., 2011. Changes in seasonal snow cover in Hindu Kush-Himalayan region. The Cryosph. Dis. 5, 755–777. https://doi.org/10.5194/tcd-5-755-2011.

Gurung, D.R., Maharjan, S.B., Shrestha, A.B., Shrestha, M.S., Bajracharya, S.R., Murthy, M.S.R., 2017. Climate and topographic controls on snow cover dynamics in the Hindu Kush Himalaya. Int. J. Climatol. 37, 3873–3882. https://doi.org/10.1002/joc.4961.

Hall, D.K., Riggs, G.A., Normalized-difference snow index (NDSI). In Encyclopedia of Snow, Ice and Glaciers; Singh, V.P., Singh, P., Haritashya, U.K., Eds.; Springer: Dordrecht, The Netherlands, 2011; pp. 779-780, ISBN 9789048126415.

Hall, D. K., Riggs, G. A., 2016. MODIS/Terra Snow Cover Daily L3 Global 500m SIN Grid, Version 6. Boulder, Colorado USA. NASA National Snow and Ice Data Centre Distributed Active Archive Center. Doi: 10.5067/MODIS/MOD10A1.006.

Hartmann, D.L., Klein, Tank, A.M.G., Rusticucci, M., Alexander, L.V., Brönnimann, S., Charabi, Y., Dentener, F.J., Dlugokencky, E.J., Easterling, D.R., Kaplan, A., Soden, B. J., Thorne, P.W., Wild, M., Zhai, P.M., Observations: atmosphere and surface. In: Climate Change 2013: The Physical Science Basis. Contribution of Working Group I to the Fifth Assessment Report of the Intergovernmental Panel on Climate Change. Stocker, T.F., D, Qin., G.-K.Plattner., M. Tignor., S.K. Allen., J, Boschung., A. Nauels., Y. Xia., V. Bex., P.M. Midgley. (Eds.) Cambridge University Press, Cambridge, United Kingdom and New York, NY, USA, pp.159–254. Doi: 10.1017/CBO9781107415324.008.

Hori., M., Sugiura, K., Kobayashi, K., et al., 2017. A 38-year (1978–2015) Northern Hemisphere daily snow cover extent product derived using consistent objective criteria from satellite-borne optical sensors. Remote Sens. of Environ. 191, 402-418. 10.1016/j.rse.2017.01.023.

Immerzeel, W.W., Lutz, A.F., Andrade, M., Bahl, A., Beimans, H., Bolch, T., Hyde, S., Brumby, S., Davis, B.J., Elmore, A.C., Feng, M., Fernandez, A., Hartiashya, U., Kargel, J.S., Koppes, M., Kraaijenbrink, P.D.A., Kulkarni, A.V., Mayerwski, P., Nepan, S., Pacheco, P., Painter, T.H., Pellicciotti, F., Rajaram, H., Rupper, S., Sinisalo, A., Shrestha, A.B., Viviroli, D., Wada, Y., Xiao, C., Yao, T., Baillie, E.M., 2020. Importance and vulnerability of the world's water towers. Nature 577, 364–369. https://doi.org/10.1038/s41586-019-1822-y.

Jain, S.K., Goswami, A., Saraf, A.K., 2009. Role of elevation and aspect in snow distribution in western Himalaya. Water Resour. Manage. 23, 71–83. https://doi.org/10.1007/s11269-008-9265-5.

Jarihani, A.A., Callow, J.N., McVicar, T.R., Van Niel, T.G., Larsen, J.R., 2015. Satellite-derived digital elevation model (DEM) selection, preparation and correction for hydrodynamic modelling in large, low-gradient and data-sparse catchments. J. Hydrol. 524, 489–506. https://doi.org/10.1016/j.jhydrol.2015.02.049.

Jasrotia, A.S., Baru, D., Kour, R., Ahmad, S., Kour, K., 2021. Hydrological modeling to simulate stream flow under changing climate conditions in Jhelum catchment, western Himalaya. J. Hydrolog. 593, 125887 https://doi.org/10.1016/j.jhydrol.2020.125887.

Karki, R., Hasson, S ul., Gerlitz, L., Talchabhadel, R., Schickhoff, U., Scholten, T., Böhner, J., 2020. Rising mean and extreme near surface air temperature across Nepal. Int. J. Climatol. 40(4), 2445-2463. Doi: 10.1002/joc.6344.

Karki, R., Hasson, S., Schickhoff, U., Scholten, T., Böhner, J., 2017. Rising Precipitation Extremes across Nepal. Climate 5, 4. https://doi.org/10.3390/cli5010004.

Kenawy, A.M., Hereher, M.E., Robba, S.M., 2019. An assessment of the accuracy of MODIS land surface temperature over Egypt using ground-based measurements. Remote Sens. 11, 2369. https://doi.org/10.3390/rs11202369.

Kour, R., Patel, N., Krishna, A.P., 2016. Effects of terrain attributes on snow-cover dynamics in parts of Chenab basin, western Himalayas. Hydro. Sci. 61 (10), 1861–1876. https://doi.org/10.1080/02626667.2015.1052815.

Krishnan, R., Shrestha, A.B., Ren, G., Rajbhandari, R., Saeed, S., Sanjay, J., Syed, M.A., Vellore, R., Xu, Y., You, Q., Ren, Y., 2019. Unravelling Climate Change in the Hindu Kush Himalaya: Rapid Warming in the Mountains and Increasing Extremes. In: Wester, P., Mishra, A., Mukherji, A., ShresthaBhakta, Arun (Eds.), The Hindu Kush Himalaya Assessment: Mountains, Climate Change, Sustainability and People. Springer International Publishing, Cham, pp. 57–97. https://doi.org/10.1007/978-3-319-92288-1_3.

Li, Y., Tao, H., Su, B., Kundzewicz, Z.W., Jiang, T., 2019. Impacts of 1.5 °C and 2 °C global warming on winter snow depth in Central Asia. Sci. Total Environ. 651, 2866–2873. https://doi.org/10.1016/j.scitotenv.2018.10.126.

Mal, S., Mehta, M., Singh, R., Schickhoff, U., Bisht, M.P.S., 2019. Recession and morphological changes of the debris-covered Milam Glacier in Gori Ganga Valley, Central Himalaya, India, Derived from Satellite Data. Front. Environ. Sci. 7, 42. https://doi.org/10.3389/fenvs.2019.00042.

Midhuna, T.M., Kumar, P., Dimri, A.P., 2020. A new Western Disturbance Index for the Indian winter monsoon. J. Earth Syst. Sci. 129, 59. https://doi.org/10.1007/s12040-019-1324-1.

Mishra, B., Babel, M.S., Tripathi, N.K., 2014. Analysis of climatic variability and snow cover in the Kaligandaki River Basin, Himalaya. Nepal. Theor. Appl. Climatol. 116, 681–694. https://doi.org/10.1007/s00704-013-0966-1.

Misra, A., Kumar, A., Bhamri, R., Haritashya, U.K., Verma, A., Dobhal, D.P., Gupta, A.K., Gupta, G., Upadhyay, R., 2020. Topographic and climatic influence on seasonal snow cover: Implications for the hydrology of ungauged Himalayan basins. India. J. Hydrolog. 585 https://doi.org/10.1016/j.jhydrol.2020.124716.

Mukhopadhyay, B., Khan, A., 2014. A quantitative assessment of the genetic sources of the hydrologic flow regimes in Upper Indus Basin and its significance in a changing climate. J. Hydrol 509, 549–572. https://doi.org/10.1016/j.jhydrol.2013.11.059.

Nepal, S., Khatiwada, K.R., Pradhananga, S., et al., 2021. Future snow projections in a small basin of the western Himalaya. Sci. Total Environ. https://doi.org/10.1016/j.scitotenv.2021.148587.

Notarnicola, C., 2020. Hotspot of snow cover changes in global mountain regions over 2000–2018. Remote. Sens. of Environ. 243, 111781 https://doi.org/10.1016/j.rse.2020.111781.

Palazzi, E., Hardeberg, J.V., Provenzale, A., 2013. Precipitation in the Hindu-Kush Karakoram Himalaya: observations and future scenarios. J. Geophys. Res. Atmos. 118, 85–100. https://doi.org/10.1029/2012JDO18697.

Pepin, N., Bradley, R.S., Diaz, H.F., Baraer, M., Caceres, E.B., Forsythe, N., Fowler, H., Greenwood, G., Hashmi, M.Z., Liu, X.D., Miller, J.R., Ning, L., Ohmura, A., Palazzi, E., Rangwala, I., Schöner, W., Severskiy, I., Shahgedanova, M., Wang, M.B., Williamson, S.N., Yang, D.Q., 2015. Elevation-dependent warming in mountain regions of the world. Nat. Clim. Chang. 5, 424–430. https://doi.org/10.1038/nclimate2563.

Sahu, N., Behera, S.K., Yamashiki, Y., Takara, K., Yamagata, T., 2012. IOD and ENSO impacts on the extreme stream-flows of Citarum river in Indonesia. Clim. Dyn. 39, 1673–1680. https://doi.org/10.1007/s00382-011-1158-2.

Sahu, R., Gupta, R.D., 2020. Snow cover area analysis and its relation with climate variability in Chandra basin, Western Himalaya, during 2001–2017 using MODIS and ERA5 data. Environ Monit Assess 192, 489. https://doi.org/10.1007/s10661-020-08442-8.

Salerno, F., Guyennon, N., Thakuri, S., Viviano, G., Romano, E., Vuillermoz, E., 2015. Weak precipitation, warm winters and springs impact glaciers of south slopes of Mt. Everest (central Himalaya) in the last 2 decades (1994–2013). Cryosphere 9, 1229–1247. https://doi.org/10.5194/tc-9-1229-2015.

Sánchez-Ruiz, S., Moreno-Martínez, A., Izquierdo-Verdiguier, E., Chiesi, M., Maseli, F., Gilabert., M.A., 2019. Growing stock volume from multi-temporal landsat imagery through google earth engine. Int J Appl Earth Obs Geoinf. 83, 101913. 10.1016/j.jag.2019.101913.

Sazib, N., Mladenova, I., Bolten, J., 2018. Leveraging the Google Earth Engine for Drought Assessment Using Global Soil Moisture Data. Remote Sens. 10, 1265. https://doi.org/10.3390/rs10081265.

Sharma, E., Molden, D., Rahman, A., et al., 2019. Introduction to the Hindu Kush Himalaya Assessment. In: Wester, P., Mishra, A., Mukherji, A., Shrestha, A.B. (Eds.), The Hindu Kush Himalaya Assessment: Mountains, Climate Change, Sustainability and People. Springer International Publishing, Cham, pp. 1–16.

Sharma, V., Mishra, V.D., Joshi, P.K., 2014. Topographic controls on spatiotemporal snow cover distribution in northwest Himalaya. Int. J Remote Sens 35 (9), 3036–3056. https://doi.org/10.1080/01431161.2014.894665.

Shrestha, N.K., Qamer, F.M., Pedreros, D., Murthy, M.R.S., Wahid, S., Shrestha, M., 2017. Evaluating the accuracy of Climate Hazard Group (CHG) satellite rainfall estimates for precipitation based drought monitoring in Koshi basin. Nepal. J. Hydrol. Reg. Stud. 13, 138–151. https://doi.org/10.1016/j.ejrh.2017.08.004.

Singh, D.K., Gusain, H.S., Mishra, V., Gupta, N., 2018. Snow cover variability in North-West Himalaya during last decade. Arab J Geosci 11, 579. https://doi.org/10.1007/s12517-018-3926-3.

Skiles, S.M., Flanner, M., Cook, J.M., Dumont, M., Painter, T.H., 2018. Radiative forcing by light-absorbing particles in snow. Nat. Clim. Chang. 8, 964–971. https://doi.org/10.1038/s41558-018-0296-5.

Snapir, B., Momblanch, A., Jain, S.K., Waine, T.W., Holman, I.P., 2019. A method for monthly mapping of wet and dry snow using Sentinel-1 and MODIS: Application to a Himalayan river basin. Int. J. Appl. Earth Obs. Geoinfo. 74, 222–230. https://doi.org/10.1016/j.jag.2018.09.011.

Stillinger, T., Roberts, D.A., Collar, N.M., Dozier, J., 2019. Cloud Masking for Landsat 8 and MODIS Terra Over Snow-Covered Terrain: Error Analysis and Spectral Similarity Between Snow and Cloud. Water Resour. Res. 55 (7), 669–6184. https://doi.org/10.1029/2019WR024932.

Tahir, K.M., Yin, Y., Wang, Y., Babar, Z.A., Yan, D., 2015. Impact assessment of orography on the extreme precipitation event of July 2010 over Pakistan: A numerical study. Adv. Meteorol. Doi: 10.1155/2015/510417.

Tahir, A.A., Chevallier, P., Arnaud, Y., Ashraf, M., Bhatti, M.T., 2015b. Snow cover trend and hydrological characteristics of the Astore River basin (Western Himalayas) and its comparison to the Hunza basin (Karakoram region). Sci. Total Environ. 505, 748–761. https://doi.org/10.1016/j.scitotenv.2014.10.065.

Tran, H., Nguyen, P., Ombadi, M., Hsu, K.L., Sorooshian, S., Qing, X., 2019. Data Descriptor: A cloud-free MODIS snow cover dataset for the contiguous United States from 2000 to 2017. Sci. Data 6, 180300. https://doi.org/10.1038/sdata.2018.300.

Ullah, W., Wang, G., Ali, G., Hagan, D.F.T., Bhatti, A.S., Lou, D., 2018. Comparing multiple precipitation products against in-situ observations over different climate regions of Pakistan. Remote Sens. 11, 628. https://doi.org/10.3390/rs11060628.

Wang, N., Lombardo, L., Gariano, S.L., Cheng, W., Liu, C., Xiong, J., Wang, R., 2021. Using satellite rainfall products to assess the triggering conditions for hydro-morphological processes in different geomorphological settings in China. Int J Appl Earth Obs Geoinf. 102, 102350 https://doi.org/10.1016/j.jag.2021.102350.

You, Q., Wu, T., Shen, L., Pepin, N., Zhang, L., Jiang, Z., Wu, Z., Kang, S., Agha Kouchak, A., 2020. Review of snow cover variation over the Tibetan Plateau and its influence on the broad climate system. Earth-Sci. Rev. 201, 103043 https://doi.org/10.1016/j.earscirev.2019.103043.